Distributed measurement of supercontinuum generation along a silica fiber taper using a confocal spectrometer

Yosri Haddad[1], Thibaut Sylvestre[1], Jean-Charles Beugnot[1], Samuel Margueron[1], and Gil Fanjoux[1,*]

[1] *Institut FEMTO-ST, CNRS UMR 6174, Université de Franche-Comté, 25030 Besançon, France*
[*] *gil.fanjoux@univ-fcomte.fr*

Compiled October 11, 2024

A highly sensitive distributed measurement technique is employed to map supercontinuum generation along a tapered silica optical fiber. This technique, which utilizes a confocal Raman micro-spectrometer, relies on analyzing far-field frequency-resolved Rayleigh scattering along the waveguide with micrometer-scale spatial resolution and high spectral resolution. Non-destructive and non-invasive, the mapping system enables observation of every stage of supercontinuum generation along the fiber cone, including cascade Raman scattering, four-wave mixing, and dispersive wave generation. Consequently, it unveils unique nonlinear spatial dynamics that are beyond the reach of standard spectral analyzers.

OCIS codes: (060.2270) Fiber characterization, (290.5870) Scattering, Rayleigh, (170.5810) Scanning microscopy

http://dx.doi.org/10.1364/ao.XX.XXXXXX

1. INTRODUCTION

Since its discovery in the early years of nonlinear optics, supercontinuum (SC) generation has continuously attracted great interest with a significant impact on both basic science and technology [1, 2]. SC light represents a unique and versatile single-point source of ultra-broadband radiation with high brightness and large coherence, finding numerous applications in diverse fields of modern optical sciences. Important applications of broadband SC sources include optical coherence tomography (OCT), fluorescence imaging, optical sensing, absorption spectroscopy, and optical frequency comb metrology [3]. Technological advances in the development of novel ultrafast laser sources, in the design and fabrication of optical fibers and on-chip integrated waveguides, foster new investigations on SC generation in various nonlinear media, and yet unexplored regions of the electromagnetic spectrum [3].

While SC light has been carefully analyzed in both the time and frequency domains, enabling close comparison to numerical simulations based on the generalized nonlinear Schrödinger equation (GNLSE) [2], its longitudinal dynamics along the waveguide remains challenging to access experimentally. There is thus a particular need for high-sensitive distributed measurement to see SC build up inside the nonlinear waveguide. This, in turn, would allow refinement and optimization of simulation parameters, including dispersion coefficients, wavelength-dependent loss, and nonlinear Kerr and Raman coefficients. Accurately mapping the longitudinal SC generation along the waveguide, especially in regions that are non-uniform or have defects, represents a valuable tool for improving multi-parameter nonlinear models, in conjunction with neural network algorithms [4].

Several distributed measurement techniques dedicated to SC analysis have already been proposed and demonstrated [5, 6]. One method is based on using a modified optical time domain reflectometer (OTDR) to map SC with meter spatial resolution [5]. Another method, potentially invasive, involves using a scanning near-field optical microscope (SNOM) for short millimeter-long waveguides with nanometer-scale resolution [6]. These techniques have enabled careful mapping of SC generation in short or long waveguides. For completeness, we can also mention the destructive cutback technique [7]. However, there is currently no distributed technique suitable for centimeter-long nonlinear waveguides, such as fiber tapers or long-spiral integrated waveguides. We recently proposed a new method based on a confocal micro-spectrometer, allowing point-to-point frequency-resolved Rayleigh scattering (RS) measurements with both micrometer spatial resolution and sub-nanometer spectral resolution [8]. We demonstrated that this method enables the measurement of Rayleigh scattering along a waveguide operating in the linear regime, and exhibits nearly the same performance as the state-of-the-art optical backscatter reflectometer (OBR) at telecom wavelength [9], or imaging system-based on EM-CCD cameras for 2D measurements [10]. The primary advantage of this technique lies in its ability to provide simultaneous hyperspectral imaging alongside high spatial resolution, enabling longitudinal measurements of the light spectrum inside the photonic waveguide.

In this paper, we applied this mapping technique to carefully characterize SC generation along a highly tapered silica optical fiber with longitudinally-varying dispersion and nonlinearity [11–14]. We observed, in particular, the gradual generation of a multi-order Raman cascade in the first taper section enhanced by four-wave mixing (FWM), and followed by the generation

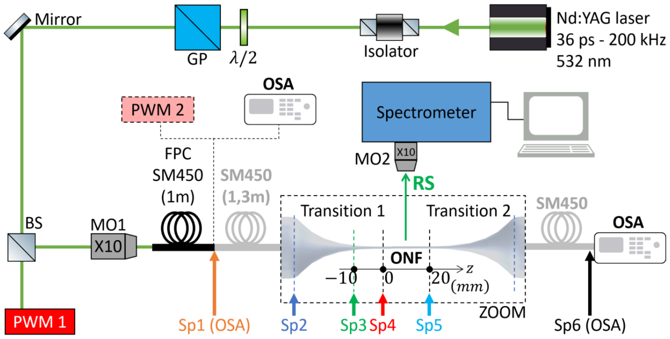

Fig. 1. Experimental setup. GP, Glan prism; BS, non-polarizing beam splitter; $\lambda/2$, half-wave plate; PWM, power meter; FPC, fiber patch cord; ONF, optical nanofiber; OSA, optical spectrum analyzer; MO1 and MO2, microscope objectives; Spi, spectrum number i; RS, Rayleigh scattering signal measured by the spectrometer.

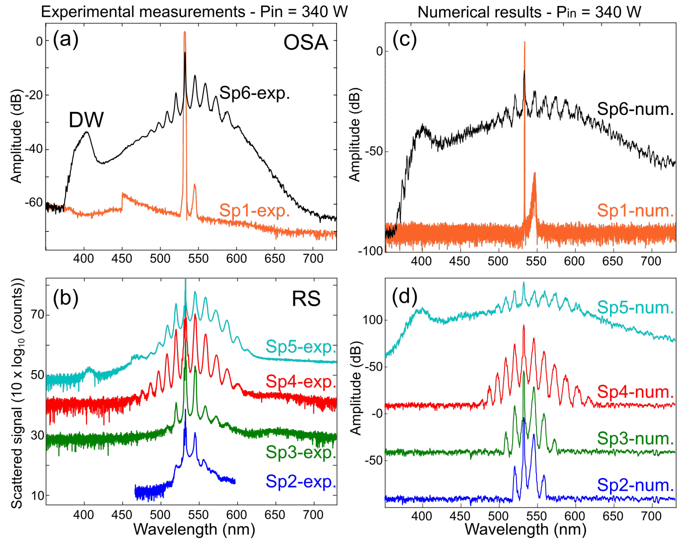

Fig. 2. (a-b) Experimental spectra and (c-d) results of numerical simulations at the input (Sp1, orange curve) and at the output (Sp6, black curve) of the fiber system, at the input of the transition 1 (Sp2, blue curve), 1 cm before the input of the ONF (Sp3, green curve), at the input of the nanofiber (Sp4, red curve), and at the end of the nanofiber (Sp5, cyan curve). Spectra in (b) and (d) are vertically shifted for clarity. DW, dispersive wave.

of dispersive waves (DW) in the taper. All experimental observations were compared to numerical simulations with very good agreement. Moreover, with access to experimental longitudinal spectral measurements, we demonstrate that accurately matching experimental spectra recorded at various propagation distances with numerical simulations demands a deeper comprehension of the nonlinear dynamics and better adjustment of physical parameters.

2. EXPERIMENTAL SETUP

The experimental setup is illustrated in Figure 1. It closely resembles the setup previously described in Ref. [8]. The key element is a confocal Raman micro-spectrometer (Monovista CRS+, S&I GmbH) used to detect the RS in the direction perpendicular to the waveguide under study. The confocal microscope part of the device is equipped with a high-precision motorized stage for the 3D displacement of the waveguide with step size and precision below 100 nm. This system provides an accurate 3D spatial trajectory all along the waveguide. The right-angle scattered light from the guided light in the optical fiber is collected using a $\times 10$ microscope objective and recorded by the spectrometer. The latter includes a 300 lines/mm diffraction grating and a back-illuminated cooled CCD detector (-85°C), enabling an ultra-low detection threshold and a high signal-to-noise ratio (SNR). The whole distributed system achieves a spatial resolution of up to 5 µm and a spectral resolution of 0.2 nm. No normalization was applied to the different scans along the fiber, except for accounting for the spectral dependency of the micro-spectrometer, which includes Rayleigh scattering and CCD detector wavelength dependency. Each measurement with our system takes about 3 minutes at the nanofiber level (Sp3 to Sp5) and 10 minutes at the standard fiber level (Sp2). This difference is due to the large scattering of the nanofiber by its surface [8, 9].

The optical nanofiber (ONF) was manufactured by heating and tapering down a standard visible single-mode fiber (Thorlabs SM450) using the heat-brush technique [13–15]. The taper diameter was accurately measured at 690 nm using a scanning electron microscope (SEM) with a uniform section over 2 cm, linked to the standard fibers by two 48 cm-long adiabatic tapered transitions [8]. The optical losses have been measured as low as 0.2 dB at 532 nm. Just after manufacturing, the taper was placed inside a closed transparent plexiglass box to protect it from external air vibrations and to avoid contamination by dust or water. A 0.5 m-long fiber patch cord (SM450) was spliced 80 cm from the taper's input (See Fig. 1). The whole fiber system was pumped with a frequency-doubled picosecond Nd:YAG laser at 532 nm, delivering a short pulse of 36 ps width at a repetition rate of 200 MHz. The pump power stability was continuously monitored using a power meter (PWM1), and the pump frequency was filtered out from the spectrometer using three Notch filters. The laser was first injected into a 1 m-long SM450 patch cord to monitor the input power (PWM2) and the input optical spectrum (Sp1 in Fig. 1). The RS measurements were carried out at four different locations along the fiber taper, denoted Sp2 to Sp5 on Fig. 1, and they were compared to standard optical spectrum analyzers (OSA, Yokogawa AQ6373) at both the fiber system input and output (Sp1 and Sp6 on Fig. 1). During our experiments, we realized that the stability of the SC was limited over time, certainly due to thermal effects at the nanofiber level. In order to achieve SC stability, controlled with the OSA at the fiber outlet, we limited the total duration of the experiments to less than one hour. This consequently limits the number of measurements.

3. EXPERIMENTAL AND NUMERICAL RESULTS

Figures 2(a) and (b) show the experimental spectra measured with the OSA (Sp1-exp and Sp6-exp) and with the confocal Raman microscope (Sp2-exp to Sp5-exp), respectively. We observe the gradual generation of cascaded Raman scattering on both Stokes and anti-Stokes sides of the pump, towards SC generation at the fiber output along with the generation of a DW near 400 nm (See black spectrum Sp6-exp). Note that the DW was detected only at the ONF output (Sp5-exp, top cyan spectrum in Fig 2(b)), meaning that it is generated in the ONF. This clearly shows the advantage of our spectral mapping method.

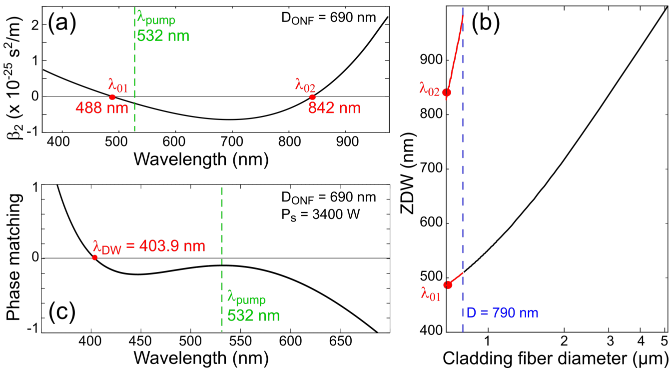

Fig. 3. (a) Group velocity dispersion β_2 versus wavelength for a fiber taper diameter of 690 nm. (b) Zero dispersion wavelengths (ZDWs) λ_{01} (black) and λ_{02} (red) as a function of fiber diameter. The vertical dashed blue line shows the fiber diameter $D = 790$ nm. (c) Phase-matching condition (Eq. 2) for dispersive wave generation versus wavelength.

To get a further understanding of the nonlinear dynamics, we numerically modeled the nonlinear pulse propagation in the fiber taper using the generalized nonlinear Schrödinger equation (GNLSE). Neglecting the self-steepening effect for picosecond pulses, this equation can be written as [2]

$$\frac{\partial A}{\partial z} + \frac{\alpha}{2}A - i\sum_{n\geq 2}^{\infty} i^{n+1}\frac{\beta_n}{n!}\frac{\partial^n A}{\partial T^n} = i\gamma(1-f_R)|A|^2 A \\ + i\gamma f_R A\int_0^{+\infty} h_R(T')\left|A(T-T')\right|^2 dT', \tag{1}$$

Where $A(z, T)$ is the complex amplitude of the electric field propagating in the z direction and in the pump velocity time frame T. β_n is the n^{th} derivative of the propagation constant β, $h_R(T)$ the delayed temporal Raman response, α the losses, and f_R the fractional contribution of the Kerr effect ($f_R = 0.18$ for standard silica fibers) [16]. The nonlinear coefficient γ was calculated as $\gamma = 2\pi n_2/(\lambda A_{eff})$ with n_2 the nonlinear index of fused silica at 532 nm and A_{eff} the effective area of the fundamental modes[16]. The dispersion coefficients β_n were derived from the effective indices n_{eff} of the fundamental mode using a finite element method (FEM) software. All these parameters were computed for each wavelength and each fiber taper diameter, taking into account the adiabatic transitions and the standard fibers [8].

Figure 3(a) shows the computed group-velocity dispersion coefficients β_2 for a taper waist of 690 nm. It features two zero dispersion wavelengths (ZDWs), $\lambda_{01} = 488$ nm and $\lambda_{02} = 842$ nm, and the dispersion is anomalous at the pump wavelength (532 nm). As the dispersion significantly varies along the fiber system, from strong normal dispersion in the standard SM450 fiber up to anomalous dispersion in the ONF, the two ZDWs significantly change longitudinally. This is illustrated in Fig 3(b) for a fiber diameter varying from 690 nm up to 5 µm. The first ZDW λ_{01} increases from 488 nm to 1000 nm and the second ZDW λ_{02} disappears from a diameter close to 790 nm. Because of the anomalous dispersion pumping regime in the ONF at 532 nm and the proximity of the pump wavelength to the first ZDW λ_{01}, the initial ps pump pulse is consequently subject to modulation instability, soliton formation and fission dynamics, along with the generation of dispersive wave (DW) due to higher-order dispersion [3]. DW frequency satisfies a phase-matching condition with the solitons, which is given by [16]

$$\beta(\omega_{DW}) - \beta(\omega_S) - (\omega_{DW} - \omega_S)/v_{g,S} - \gamma P_s/2 = 0, \tag{2}$$

with $\beta(\omega_{DW})$ and $\beta(\omega_S)$ the propagation constants of the DW and the solitons, ω_{DW} and ω_S the DW and soliton angular frequencies, $v_{g,S}$ is the soliton group velocity, P_s the soliton peak power, respectively. ω_S was set to the pump frequency ω_P, as no significant soliton self-frequency shift was experimentally and numerically observed. Figure 3(c) shows the phase-matching curve satisfying a DW wavelength at 403.9 nm for a mean soliton peak power $P_s = 3400$ W, estimated from numerical simulations. This is in quite good agreement with the experimental observations of Figs 2(a) and (b), which show a DW at around 405 nm.

We used the split-step method to solve Eq.(1) assuming all varying dispersion and nonlinear coefficients, including both linear and local losses. Figures 2(c) and (d) show the results of numerical simulations at the same locations (Spi) as in the experiment for a direct comparison. As can be seen, we get nearly the same spectral dynamics as the experiment, with the increasing cascaded Raman scattering and the DW generation at around 400 nm.

4. ANALYSIS AND DISCUSSION

We will now describe in more detail the observed and simulated spectra of Figs 2(a-d). First, the orange spectrum Sp1-exp in Fig. 2(a) shows that a first Raman Stokes order is generated in the 1 m-long SM450 patch cord, as the Sp1-num numerical spectrum of Fig. 2(c) simulated with the same peak power $P_{in} =$ 340 W. Then, the blue spectrum Sp2-exp in Fig. 2(b) shows that a weakly-developed Raman cascade is already present at the taper's input, with two Raman Stokes orders and one anti-Stokes order. The latter is generated by four-wave mixing (FWM) and its maximum intensity depends on the phase mismatch due to dispersion. This explains the large difference in intensity between the Raman Stokes and anti-Stokes orders ($\approx$ 15 dB). The numerical spectrum Sp2-num in Fig. 2(d) shows a similar behavior.

One centimeter before the end of transition 1, Sp3-exp in Fig. 2(b) shows the weak development of the Raman cascade on the Stokes side. At this location, the fiber diameter is 1.53 µm and the ZDW λ_{01} is about 665 nm (See Fig. 3(c)). This decrease of λ_{01} and the dispersion explains the difference of intensity between Stokes and anti-Stokes orders coupled by FWM, compared to Sp2-num. To get good agreement with the numerical spectrum (Sp3-num), we added an attenuation factor around 2.2 dB at the transition 1 input. This additional loss can be explained by the losses of about 2.5 dB experimentally measured in the nonlinear regime, related to the observation of light rings scattered outside the fiber at the level of the transition 1, certainly due to higher-order leaky modes. This point is important because it shows that the distributed experimental measurements allow for optimizing and refining all the numerical parameters along the waveguide used for simulations, which is not possible when using OSA measurements only.

At the end of transition 1, the spectrum Sp4-exp in Fig. 2(b) clearly shows a development of the Raman cascade on the Stokes side compared to Sp3-exp, and also more surprisingly a large development on the anti-Stokes side. This is due to the sweep of the ZDW λ_{01} from 665 nm to 488 nm, i.e. (See Fig. 3(c)), in the spectral range where the pump at 532 nm and spectral components of the Raman cascade are present. The phase mismatch

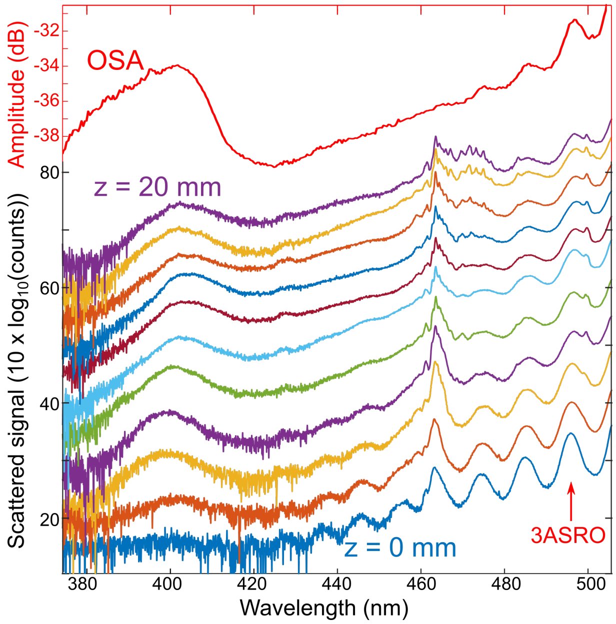

Fig. 4. Experimental spectra. Top spectrum: OSA measurement at the end of the fiber system. Bottom spectra: RS measurements along the ONF every 2 mm from $z = 0$ mm to $z = 20$ mm. 3ASRO = third anti-Stokes Raman order. Spectra are vertically shifted for clarity.

due to dispersion between Stokes and anti-Stokes peaks correspondingly decreases, which further enhances FWM efficiency towards the anti-Stokes components. The Stokes/anti-Stokes intensity difference has therefore decreased. This specific behavior is also numerically predicted in Fig. 2(d) (See Sp4-num spectrum). Each Raman Stokes and anti-Stokes order pair has slightly different intensities. Consequently, the anti-Stokes Raman cascade is highly developed as the Stokes one, which is quite remarkable in nonlinear fiber optics.

After propagation in the uniform taper, the spectrum Sp5-exp in Fig. 2(b) shows a broad DW centered at around 405 nm, in good agreement with the analytical prediction shown in Fig. 3(c). The anti-Stokes Raman cascade is also well developed and a SC begins to be generated. Numerically, the DW is centered at around 400 nm (See Sp5-num in (Fig. 2(d) at the output of the ONF, and Sp6-num in Fig. 2(c) at the output of the fiber system).

Lastly, no drastic change is observable between the output of the ONF and the output of the fiber system (Sp5-num and Sp6-num, respectively). This means that transition 2 does not significantly impact the nonlinear spectral dynamics. This is because the nonlinear coefficient strongly decreases and the dispersion increases as well.

To get further experimental details, we measured with an improved signal-to-noise ratio the anti-Stokes side of the SC spectrum from 374 nm to 506 nm, only along the 20-mm long uniform waist, where the RS signal is the highest [8, 9]. Figure 4 shows 10 RS successive spectra along the taper from $z = 0$ mm to $z = 20$ mm with a step size of 2 mm ($\approx$ 3.5 minutes per spectrum), while the top red spectrum was measured at the same time using the OSA. In Figure 4, at the beginning of the ONF ($z = 0$ mm position), the anti-Stokes Raman cascade is clearly visible up to the tenth order, and the DW is not yet observable by our system. The DW is observable from 2 mm of propagation, and its level increases along the ONF. Moreover, the anti-Stokes Raman cascade is smoothed by SC generation. We can also see in Figure 4 that the DW central frequency shifts along the ONF. This unexpected behavior is actually due to the weak SC instability over time, also seen in the OSA measurements. Another point is that weak narrow peaks appear in the spectra of Fig. 4, in the range $460 - 480$ nm from about 14 mm in the ONF, while these peaks are not observable on the OSA measurements. These peaks could be generated by interference due to dispersion, as they are close to the first ZDW (λ_{01} =488 nm).

It should be noted that, although this distributed measurement offers a micrometric spatial resolution [8], here we have only shown SC measurements with a spatial step of 2 mm, which is enough to see spectral changes seen in Fig. 4. Actually, due to localized thermal effects leading to temperature variations along the ONF and the transitions [17] because operating at 532 nm in the picosecond regime, the SC exhibits a certain instability over time. Consequently, in order to ensure SC stability during measurements, we limit the total duration at about half an hour and therefore the number of measurement points. Nevertheless, it is obvious that the micrometric spatial step can be used along an optical waveguide that presents longitudinal spectra stable over time, allowing therefore a complete mapping of the SC generation.

The problem of SC instability over time could be solved by using a pulse duration in the femtosecond range. Indeed, the energy per pulse would be lower than in the picosecond regime and should reduce thermal effects. Now, to maintain a sufficient number of photons per second to be able to detect scattered signals with our method, the repetition rate of the laser source frequency should be increased.

5. CONCLUSION

In summary, we have developed a reliable method for frequency-resolved distributed optical measurement of supercontinuum generation along an optical waveguide. The method is based on hyperspectral Rayleigh scattering analysis using a confocal Raman microscope. This non-invasive and non-destructive technique allowed us to accurately analyze nonlinear effects and supercontinuum generation along a silica-glass tapered optical fiber with micrometer spatial resolution and sub-nanometer spectral resolution.

We observed specific spectral features inside the fiber taper that were not discernible with standard spectral analysis. Furthermore, we found good agreement with numerical simulations, providing explanations for these features. From a broader perspective, this technique opens new avenues for observing localized nonlinear phenomena inside photonic waveguides. It could also be used to map nonlinear effects in other photonic platforms such as photonic integrated circuits (PICs) or photonic crystal fibers.

FUNDING ACKNOWLEDGEMENTS

This project has received funding from the Agence Nationale de la Recherche (ANR) (ANR-16-CE24-0010, ANR-15-IDEX-0003, EUR EIPHI Graduate School ANR-17-EURE-0002), the Bourgogne Franche-Comté Region, and the Horizon Europe Framework Programme (VISUAL Action 101135904).

DISCLOSURES

The authors declare that there are no conflicts of interest related to this article.

DATA AVAILABILITY STATEMENT

The data is available from the corresponding author under reasonable request.

AUTHORS CONTRIBUTION STATEMENT

Y. H. carried out the experiments and numerical simulations, T. S. participated in the theoretical analysis and understanding of nonlinear processes, J.-C. B. participated in the fabrication of the ONFs, S. M. assisted with the instrumentation and optimized the experiments based on the confocal Raman microspectrometer, G. F. initiated the idea of distributed measurements and supervised the project.

REFERENCES

1. R. R. Alfano, *The supercontinuum laser source: the ultimate white light* (Springer Nature Switzerland, 2022).
2. J. M. Dudley and J. R. Taylor, *Supercontinuum generation in optical fibers* (Cambridge University Press, Cambridge, 2010).
3. T. Sylvestre, E. Genier, A. N. Ghosh, P. Bowen, G. Genty, J. Troles, A. Mussot, A. C. Peacock, M. Klimczak, A. M. Heidt *et al.*, JOSA.B **38**, F90 (2021).
4. L. Salmela, M. Hary, M. Mabed, A. Foi, J. M. Dudley, and G. Genty, Opt. Lett. **47**, 802 (2022).
5. R. Hontinfinde, S. Coulibaly, P. Megret, M. Taki, and M. Wuilpart, Opt. letters **42**, 1716 (2017).
6. A. Coillet, M. Meisterhans, J.-B. Jager, M. Petit, J.-B. Dory, P. Noé, P. Grelu, and B. Cluzel, "Near-field imaging of octave-spanning supercontinua generation in silicon nitride waveguides (Conference Presentation)," in *Nanophotonics,* (SPIE, Strasbourg, France, 2018), p. 106720L.
7. C. Billet, J. M. Dudley, N. Joly, and J. Knight, Opt. express **13**, 3236 (2005).
8. Y. Haddad, J. Chrétien, J.-C. Beugnot, A. Godet, K. Phan-Huy, S. Margueron, and G. Fanjoux, Opt. Express **29**, 39159 (2021).
9. Y.-H. Lai, K. Y. Yang, M.-G. Suh, and K. J. Vahala, Opt. Exp. **25**, 22312 (2017).
10. J. E. Hoffman, F. K. Fatemi, G. Beadie, S. L. Rolston, and L. A. Orozco, Optica **2**, 416 (2015).
11. T. Birks, W. Wadsworth, and P. S. J. Russell, Opt. Lett. **25**, 1415 (2000).
12. L. Tong, R. R. Gattass, J. B. Ashcom, S. He, J. Lou, M. Shen, I. Maxwell, and E. Mazur, Nature **426**, 816 (2003).
13. L. Tong and M. Sumetsky, *Subwavelength and nanometer diameter optical fibers* (Springer Science & Business Media, Springer Berlin, Heidelberg, 2011).
14. A. Godet, A. Ndao, T. Sylvestre, V. Pecheur, S. Lebrun, G. Pauliat, J.-C. Beugnot, and K. P. Huy, Optica **4**, 1232 (2017).
15. L. Shan, G. Pauliat, G. Vienne, L. Tong, and S. Lebrun, Appl. Phys. Lett. **102**, 201110 (2013).
16. G. P. Agrawal, *Nonlinear Fiber Optics, fifth edition* (Elsevier & Academic Press, Oxford, 2013).
17. J. Zhang, Y. Kang, X. Guo, Y. Li, K. Liu, Y. Xie, H. Wu, D. Cai, J. Gong, Z. Shi *et al.*, Light. Sci. & Appl. **12**, 89 (2023).

FULL REFERENCES

1. R. R. Alfano, *The supercontinuum laser source: the ultimate white light* (Springer Nature Switzerland, 2022).
2. J. M. Dudley and J. R. Taylor, *Supercontinuum generation in optical fibers* (Cambridge University Press, Cambridge, 2010).
3. T. Sylvestre, E. Genier, A. N. Ghosh, P. Bowen, G. Genty, J. Troles, A. Mussot, A. C. Peacock, M. Klimczak, A. M. Heidt *et al.*, "Recent advances in supercontinuum generation in specialty optical fibers," JOSA.B **38**, F90–F103 (2021).
4. L. Salmela, M. Hary, M. Mabed, A. Foi, J. M. Dudley, and G. Genty, "Feed-forward neural network as nonlinear dynamics integrator for supercontinuum generation," Opt. Lett. **47**, 802–805 (2022).
5. R. Hontinfinde, S. Coulibaly, P. Megret, M. Taki, and M. Wuilpart, "Non-destructive distributed measurement of supercontinuum generation along highly nonlinear optical fibers," Opt. letters **42**, 1716–1719 (2017).
6. A. Coillet, M. Meisterhans, J.-B. Jager, M. Petit, J.-B. Dory, P. Noé, P. Grelu, and B. Cluzel, "Near-field imaging of octave-spanning supercontinua generation in silicon nitride waveguides (Conference Presentation)," in *Nanophotonics,* (SPIE, Strasbourg, France, 2018), p. 106720L.
7. C. Billet, J. M. Dudley, N. Joly, and J. Knight, "Intermediate asymptotic evolution and photonic bandgap fiber compression of optical similaritons around 1550 nm," Opt. express **13**, 3236–3241 (2005).
8. Y. Haddad, J. Chrétien, J.-C. Beugnot, A. Godet, K. Phan-Huy, S. Margueron, and G. Fanjoux, "Microscopic imaging along tapered optical fibers by right-angle rayleigh light scattering in linear and nonlinear regime," Opt. Express **29**, 39159–39172 (2021).
9. Y.-H. Lai, K. Y. Yang, M.-G. Suh, and K. J. Vahala, "Fiber taper characterization by optical backscattering reflectometry," Opt. Exp. **25**, 22312–22327 (2017).
10. J. E. Hoffman, F. K. Fatemi, G. Beadie, S. L. Rolston, and L. A. Orozco, "Rayleigh scattering in an optical nanofiber as a probe of higher-order mode propagation," Optica **2**, 416–423 (2015).
11. T. Birks, W. Wadsworth, and P. S. J. Russell, "Supercontinuum generation in tapered fibers," Opt. Lett. **25**, 1415–1417 (2000).
12. L. Tong, R. R. Gattass, J. B. Ashcom, S. He, J. Lou, M. Shen, I. Maxwell, and E. Mazur, "Subwavelength-diameter silica wires for low-loss optical wave guiding," Nature **426**, 816–819 (2003).
13. L. Tong and M. Sumetsky, *Subwavelength and nanometer diameter optical fibers* (Springer Science & Business Media, Springer Berlin, Heidelberg, 2011).
14. A. Godet, A. Ndao, T. Sylvestre, V. Pecheur, S. Lebrun, G. Pauliat, J.-C. Beugnot, and K. P. Huy, "Brillouin spectroscopy of optical microfibers and nanofibers," Optica **4**, 1232–1238 (2017).
15. L. Shan, G. Pauliat, G. Vienne, L. Tong, and S. Lebrun, "Stimulated raman scattering in the evanescent field of liquid immersed tapered nanofibers," Appl. Phys. Lett. **102**, 201110 (2013).
16. G. P. Agrawal, *Nonlinear Fiber Optics, fifth edition* (Elsevier & Academic Press, Oxford, 2013).
17. J. Zhang, Y. Kang, X. Guo, Y. Li, K. Liu, Y. Xie, H. Wu, D. Cai, J. Gong, Z. Shi *et al.*, "High-power continuous-wave optical waveguiding in a silica micro/nanofibre," Light. Sci. & Appl. **12**, 89 (2023).